Polar magneto-optics in simple ultrathin-magnetic-film structures

Š. Višňovský, M. Nývlt, V. Prosser, R. Lopušník, and R. Urban
Institute of Physics, Charles University, Ke Karlovu 5, 12116 Prague 2, Czech Republic

J. Ferré and G. Pénissard
Laboratoire de Physique des Solides, Associé au CNRS, Bâtiment 510, Université Paris-Sud, 91405 Orsay, France

D. Renard
Institut d'Optique Théorique et Appliquée, Associé au CNRS, Bâtiment 503, Université Paris-Sud, 91405 Orsay, France

R. Krishnan
Laboratoire de Magnétisme et Matériaux Magnétiques, CNRS, 92195 Meudon, France
(Received 13 January 1995; revised manuscript received 17 March 1995)

For a better understanding of optical interactions in magnetic layered structures we establish general expressions of both polar Kerr and Faraday first-order magneto-optical (MO) effects. The approach presented here enables the MO response of an arbitrary magnetic layer system to be analytically expressed with an accuracy practically equal (less than 10^{-4} deg) to that of the full matrix calculations usually employed for modeling MO effects in magnetic multilayers. The formulas for any particular structure are obtained from general MO expressions by introducing associated reflection and transmission coefficients. This procedure is justified here in the simple case of an ultrathin magnetic film sandwiched between two nonmagnetic layers. These accurate expressions are further simplified for ultrathin magnetic films and the limitations of this approximation discussed. The simplified formulas are then used to analyze MO polar Kerr and Faraday data in well-defined Au (5 nm)/Co/Au (25 nm) structures, grown on float glass substrates. The Co layer thicknesses are chosen in the range 0.4–2.0 nm to preserve a perpendicular magnetic anisotropy. The simplified expressions, as well as the numerical modeling of the trends in MO spectra with a variation of the overlayer or buffer layer thicknesses, show that the shape of the polar Kerr effect spectrum is mainly dependent upon the optical properties of the Au buffer layer whereas the observed MO amplitudes are reduced consistently with the absorption of the Au overlayer.

INTRODUCTION

Ultrathin film structures with a 3*d* ferromagnetic metal layer sandwiched between nonmagnetic metal layers have recently attracted considerable attention[1–4] because they serve as model systems for stabilizing new structural metallic phases or studying the origin of the interface magnetic anisotropy[1,2,5–7] and the existence and properties of magnetic domain structures.[8,9] In magnetic bilayer systems it is of interest to study the recently discovered oscillatory coupling through a nonmagnetic layer[10–13] and the giant magnetoresistance.[14–17] All these properties can be generally better analyzed in such simple magnetic structures than in multilayers.

Magneto-optics is now recognized as a very powerful technique to measure the weak magnetization of ultrathin films in both *ex situ* and *in situ* conditions.[2,18,19] MO polar Kerr and Faraday[2,20] rotation or ellipticity measuring the out-of-plane component of the magnetization are suitable for magnetic films with perpendicular magnetic anisotropy. So, the predictions of both light reflection and transmission MO measurements on ultrathin films are reported and analyzed in the present study.

From a careful analysis of MO spectroscopic measurements useful information on the modifications of the electronic structure of the magnetic metal in ultrathin metallic layers and on interactions with neighboring layers can also be deduced. Simple ultrathin film structures are again more suitable than multilayers for this purpose since the interface roughness generally increases with the number of deposited layers.[21]

MO calculations in thin magnetic film structures, based on the electromagnetic theory,[22–26] using bulklike optical and magneto-optical constants, can generally interpret well the experimental data of nearly ideal systems with steplike interfaces.

The matrix formalisms based on Maxwell theory provide good computer modeling of the MO response for a given structure. However, with such a *numerical* method it is *difficult* to handle the dependence of the MO effects on parameters characterizing the different layers. *Analytical expressions* would be more useful for the *understanding* of the MO effects in simple structures. Analytical expressions are also interesting for *fitting* experimental data, for example when looking at the fine variation of the MO effects with layer thicknesses or with values of the optical parameters.[27]

Theoretical expressions have only been proposed for understanding the polar Kerr effect in an ultrathin film

deposited on a thick buffer or for multilayers composed of ultrathin layers.[28–30,25,31] However, in many usual cases the buffer layer cannot be assumed to have an infinite thickness and for *ex situ* measurements a rather thick protective overlayer is needed. Moreover, previous expressions were only deduced for particular structures or assuming an approximation of ultrathin layers[29] for the full structure, which is not always valid.

Starting from the full matrix formalism, in the present paper we derive *exact* (accuracy better than 10^{-4} deg) *general formulas* for complex polar Kerr and Faraday effects in magnetic layered structures. This easy to use theoretical method provides rapidly the analytical expressions for the MO effects in any arbitrary layered system. The exact formulas allow us to express explicitly the dependence of the MO effects on the relevant parameters of the layered structure (i.e., thicknesses, diagonal, and off-diagonal tensor elements of each individual layer). Such general and accurate analytical approach has not been presented so far.

The general expressions are further simplified using an ultrathin-magnetic-film approximation. The validity of this approximation is discussed. We show how the proposed theory enables us to follow the development of the MO response, when the system is *built up*. The *step by step* procedure accounting for the effect of layers successively added to the structure allows important MO features to be extracted and understood.

As far as we know, up to now there is no simple and consistent approach which considers the interaction of a quasimonochromatic light within a layered structure deposited on a thick transparent substrate displaying a MO behavior. This topic is also treated in the present paper.

To check our calculations and the validity of the approximations we performed spectroscopic experiments in well characterized Au/Co/Au/ *float glass* thin-film structures with abrupt interfaces, both in MO polar Kerr and Faraday configurations. Since this well-defined system was found to be very suitable for the studies of MO interactions, we report here on a large extension of our former spectroscopic studies[32,33] to discuss the agreement with the proposed theory, especially in the Au plasma edge region, where drastic changes of the optical parameters occur. The trends in the spectra of polar Kerr and Faraday effects with the thicknesses of all layers are discussed within the simplified analytical expressions derived for the sandwich structure.

The article is organized as follows. From the full matrix formalism we first derive in Sec. I general analytical expressions for the MO effects in layered structures containing one magnetic layer and show, how to apply them to magnetic multilayers. Then application to simple sandwich structures is given and the procedure for evaluating the optical response of the sample including noncoherent light interaction in the thick glass substrate presented. Section II reports on the sample preparation and properties, on the MO experimental technique, and summarizes the theoretical procedures, including the choice of optical and MO constants used in the modeling. In Sec. III the experimental results are analyzed and discussed. Conclusions are presented in Sec. IV.

I. MAGNETO-OPTICAL CALCULATIONS

A. Yeh's formalism

The optical response of layered magnetic systems in the most general case can be appropriately modeled with a 4×4 matrix formalism, based on the approach developed by Yeh.[22,23] Here we restrict our investigations to perpendicularly ($\|z$) magnetized layered structures characterized by the complex permittivity tensor

$$\overleftrightarrow{\varepsilon}=\begin{bmatrix}\varepsilon_{xx} & \varepsilon_{xy} & 0\\ -\varepsilon_{xy} & \varepsilon_{xx} & 0\\ 0 & 0 & \varepsilon_{zz}\end{bmatrix} . \tag{1}$$

Considering the case of normal light incidence, it is straightforward to demonstrate that the proper modes are circularly polarized and associated to complex refractive indices $N^{\pm}$, defined as

$$(N^{\pm})^2=(n^{\pm}-ik^{\pm})^2=\varepsilon_{xx}\pm i\varepsilon_{xy} . \tag{2}$$

The transfer matrix $\mathbf{M}$ of a structure consisting of m layers, which relates the field components of the optical wave in the two external half-spaces, is block diagonal[23] because there is no interaction between right circularly polarized (RCP) and left circularly polarized (LCP) proper modes. Thus we can calculate the optical response of the layered structure using two 2×2 matrices for incident RCP ($\mathbf{M}^{+}$) and LCP ($\mathbf{M}^{-}$) waves

$$\mathbf{M}^{\pm}=\prod_{n=1}^{m+1}\mathbf{T}^{\pm}_{n-1,n}=\begin{bmatrix}M^{\pm}_{11} & M^{\pm}_{12}\\ M^{\pm}_{21} & M^{\pm}_{22}\end{bmatrix} . \tag{3}$$

Here $\mathbf{T}^{\pm}_{n-1,n}$ are the transfer matrices which relate the electric and magnetic-field amplitudes in the $(n-1)$th layer at the interface between the $(n-1)$th and nth layers with those in the nth layer at the interface between the nth and $(n+1)$th layers. The first component of the field amplitude vector corresponds to the wave propagating from the medium n to $n+1$, the second one corresponds to the wave with a complex wave vector having the same magnitude but with an opposite orientation. In the special case of polar magnetization and normal light incidence the transfer matrices can be expressed in terms of the reflection r_{kl} and transmission $\mathbf{t}_{kl}$ coefficients at the kl interfaces

$$r_{kl}=\frac{N_k-N_l}{N_k+N_l} , \tag{4a}$$

$$\mathbf{t}_{kl}=1+r_{kl} . \tag{4b}$$

Thus one can finally write[34]

$$\mathbf{T}^{\pm}_{n-1,n}=\frac{1}{\mathbf{t}^{\pm}_{n-1,n}}\times\begin{bmatrix}e^{i\gamma N_n^{\pm}t_n} & r^{\pm}_{n-1,n}e^{-i\gamma N_n^{\pm}t_n}\\ r^{\pm}_{n-1,n}e^{i\gamma N_n^{\pm}t_n} & e^{-i\gamma N_n^{\pm}t_n}\end{bmatrix} . \tag{5}$$

Here γ is the magnitude of the radiation wave vector in

vacuum, t_n and $N_n^{\pm}$ stand for the thickness and the complex refractive indices for RCP (+) and LCP (−) waves of the nth layer. The exponential factors in Eq. (5) characterize the transformation of the waves during the propagation in the layer n. In the last matrix $\mathbf{T}^{\pm}_{m,m+1}$ of the product in Eq. (3) we usually set $t_{m+1}=0$. In this case the $\mathbf{M}^{\pm}$ matrices relate the field components in the isotropic half-spaces at the interfaces with the first and the last layers.

The optical response of the layered structure is determined by reflection and transmission coefficients for RCP and LCP waves

$$r^{\pm}=\frac{M^{\pm}_{21}}{M^{\pm}_{11}} , \tag{6a}$$

$$\mathbf{t}^{\pm}=\frac{1}{M^{\pm}_{11}} . \tag{6b}$$

Note that for a nonmagnetized multilayer the off-diagonal permittivity tensor elements vanish; then $r^{\pm}=r$ and $\mathbf{t}^{\pm}=\mathbf{t}$.

After transmission through the sample or reflection at its surface an incident linearly polarized light beam is generally transformed into an elliptically polarized wave, for which one can define[35] the rotation θ of its principal axis and its ellipticity ϵ. This allows the magneto-optical observables to be expressed. In light reflection the polar Kerr rotation (PKR) θ_K and the ellipticity (PKE) ϵ_K can be defined as

$$\theta_K=\frac{1}{2}\arg\left[\frac{r^-}{r^+}\right] , \tag{7a}$$

$$\tan\epsilon_K=\frac{|r^-|-|r^+|}{|r^-|+|r^+|} , \tag{7b}$$

while in light transmission the Faraday rotation (FR) θ_F and the ellipticity (FE) ϵ_F express as

$$\theta_F=\frac{1}{2}\arg\left[\frac{\mathbf{t}^-}{\mathbf{t}^+}\right] , \tag{8a}$$

$$\tan\epsilon_F=-\frac{|\mathbf{t}^-|-|\mathbf{t}^+|}{|\mathbf{t}^-|+|\mathbf{t}^+|} . \tag{8b}$$

Note that the signs of MO observables are a matter of sign convention.[36]

Modeling of the optical response of layered structures, based on the proposed matrix formalism, is quite simple and remarkably efficient especially for complicated structures; the addition of one layer corresponds to the addition of one transfer matrix into the matrix multiplication procedure.

B. General analytical expressions for MO effects in thin film structures

General expressions for the MO complex polar Kerr effect (CPKE) Φ_K and complex Faraday effect (CFE) Φ_F will be derived from the full matrix formalism.[23] Two assumptions are fulfilled in thin magnetic-film structures: (a) the approximation of small ellipsometric angles, leading to

$$\Phi_K=\theta_K-i\epsilon_K\approx i\frac{r^+-r^-}{r^++r^-} , \tag{9a}$$

$$\Phi_F=\theta_F+i\epsilon_F\approx i\frac{\mathbf{t}^+-\mathbf{t}^-}{\mathbf{t}^++\mathbf{t}^-} , \tag{9b}$$

and (b) the restriction to linear MO effects with the complex circular birefringence $\Delta N=\frac{1}{2}(N^+-N^-)$.

We present here an approach for determining the MO response of a layered structure containing η magnetic layers displaying only the above approximations. The quantities (r^+-r^-) and $(\mathbf{t}^+-\mathbf{t}^-)$ may be (for first-order MO effects) expressed by the total differentials in r and $\mathbf{t}$, with respect to the magnetic circular birefringences of all magnetic layers. From Eqs. (9a) and (9b) the CPKE and CFE expressions can be written as

$$\Phi_K=\frac{i}{r}\sum_{j=1}^{\eta}\frac{\partial r}{\partial N_j}\Delta N_j , \tag{10a}$$

$$\Phi_F=\frac{i}{\mathbf{t}}\sum_{j=1}^{\eta}\frac{\partial t}{\partial N_j}\Delta N_j . \tag{10b}$$

In other words the MO response of the whole structure obeys the principle of superposition and may be expressed as a summation over contributions of all individual magnetic layers. Each term j can be evaluated considering that only the layer j remains magnetically active in the structure, i.e., $\Delta N_j\neq 0$ and $\Delta N_{k(\neq j)}\equiv 0$. All these terms are obtained from the derivative of the reflection and transmission coefficients of the nonmagnetized multilayer, r and $\mathbf{t}$, which can be calculated from Eqs. (6), writing $r=r^{\pm}$ and $\mathbf{t}=\mathbf{t}^{\pm}$, respectively, or using any other matrix or iterative procedure.[35]

As we will show later, it turns out that a jth component in Eqs. (10) can always be written as a sum of two terms

$$\Delta N_j\, A\, 2i\gamma N_j t_j+\Delta N_j B(e^{-2i\gamma N_j t_j}-1) ,$$

where A and B are complex coefficients. Using this approach the quantities Φ_K and Φ_F can be calculated with an *accuracy* which in practice *is equal* to that of the full matrix formalism.

1. *The effective interfaces method*

Now the Yeh formalism, is applied to develop a method which can be successfully used for obtaining general analytical expressions of MO effects in magnetic layered structures. The principle of linear superposition [Eqs. (10)] being demonstrated, we will consider first the case of a multilayer with only one magnetically active layer.

The effective interfaces method presented here is based on the equivalence between a layered structure containing one magnetic layer and the same single magnetic layer with *effective interfaces* characterized by reflection and transmission coefficients which represent the optical behavior of the other layers (Fig. 1).

To obtain these generalized coefficients we introduce, as in Eq. (3), more general matrices $\mathbf{M}^{\pm}_{IJ}$ which relate the electric-field amplitudes in two media I and J at the inter-

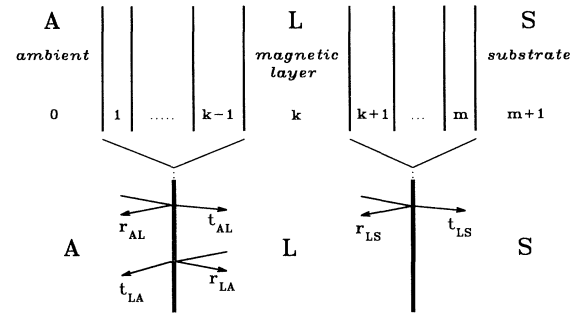

FIG. 1. Cross section of a structure composed of m layers, inserted between an ambient medium A and a semi-infinite nonmagnetic substrate S, where only the layer k is supposed to be magnetically active. This system is represented by an equivalent structure consisting of the ambient medium A, the magnetic layer L and the substrate S, with effective interfaces characterized by the reflection and transmission coefficients of the (1 to $k-1$) and ($k+1$ to m) stacks of nonmagnetic layers.

faces with a stack of layers inserted between them. This stack, replaced in the proposed approach by an effective interface, is then characterized by reflection and transmission coefficients defined by the following equations:

$$\begin{bmatrix} 1 \\ r_{IJ}^{\pm} \end{bmatrix} = \mathbf{M}_{IJ}^{\pm} \begin{bmatrix} \mathbf{t}_{IJ}^{\pm} \\ 0 \end{bmatrix} , \tag{11a}$$

$$\begin{bmatrix} 0 \\ \mathbf{t}_{JI}^{\pm} \end{bmatrix} = \mathbf{M}_{IJ}^{\pm} \begin{bmatrix} r_{JI}^{\pm} \\ 1 \end{bmatrix} , \tag{11b}$$

where the vectors on the left- (right-) hand side of Eqs. (11) correspond to the $I(J)$ medium. From Eqs. (11) one obtains

$$r_{IJ}^{\pm} = \frac{M_{21}^{\pm}}{M_{11}^{\pm}} , \tag{12a}$$

$$\mathbf{t}_{IJ}^{\pm} = (M_{11}^{\pm})^{-1} , \tag{12b}$$

$$r_{JI}^{\pm} = -\frac{M_{12}^{\pm}}{M_{11}^{\pm}} , \tag{12c}$$

$$\mathbf{t}_{JI}^{\pm} = M_{22}^{\pm} + M_{21}^{\pm} r_{JI}^{\pm} . \tag{12d}$$

These equations enable the matrices $\mathbf{M}_{IJ}^{\pm}$ to be expressed in terms of the reflection and transmission coefficients

$$\mathbf{M}_{IJ}^{\pm} = \frac{1}{\mathbf{t}_{IJ}^{\pm}} \begin{bmatrix} 1 & -r_{JI}^{\pm} \\ r_{IJ}^{\pm} & \Psi_{IJ}^{\pm} \end{bmatrix} , \tag{13}$$

where

$$\Psi_{IJ}^{\pm} = \mathbf{t}_{IJ}^{\pm} \mathbf{t}_{JI}^{\pm} - r_{IJ}^{\pm} r_{JI}^{\pm} . \tag{14}$$

Note that for a single interface between I and J media the matrices $\mathbf{M}_{IJ}^{\pm}$ are reduced to the usual transfer matrices [Eq. (5)] for $t_J = 0$.

Then the optical response of the system consisting of m layers inserted between two isotropic half-spaces "A" (medium 0) and "S" (medium $m+1$) is described by the matrices $\mathbf{M}_{AS}^{\pm}$ (Fig. 1). Let us name "L" the kth ($1 \le k \le m$) layer. Similarly to Eq. (3) the matrix $\mathbf{M}_{AS}^{\pm}$ can be expressed as a product

$$\mathbf{M}_{AS}^{\pm} = \mathbf{M}_{AL}^{\pm} \begin{bmatrix} e^{i\gamma N_L^{\pm} t_L} & 0 \\ 0 & e^{-i\gamma N_L^{\pm} t_L} \end{bmatrix} \mathbf{M}_{LS}^{\pm} , \tag{15}$$

with matrices

$$\mathbf{M}_{AL}^{\pm} = \prod_{n=1}^{k} T_{n-1,n}^{\pm} = \frac{1}{\mathbf{t}_{AL}^{\pm}} \begin{bmatrix} 1 & -r_{LA}^{\pm} \\ r_{AL}^{\pm} & \Psi_{AL}^{\pm} \end{bmatrix} , \tag{16}$$

$$\mathbf{M}_{LS}^{\pm} = \prod_{n=k+1}^{m+1} T_{n-1,n}^{\pm} = \frac{1}{\mathbf{t}_{LS}^{\pm}} \begin{bmatrix} 1 & -r_{SL}^{\pm} \\ r_{LS}^{\pm} & \Psi_{LS}^{\pm} \end{bmatrix} . \tag{17}$$

It should be pointed out that the transfer matrices $T_{k-1,k}^{\pm}$ and $T_{m,m+1}^{\pm}$ are calculated taking $t_k = 0$ and $t_{m+1} = 0$, respectively.

The reflection and transmission coefficients of the full layered structure, shown in Fig. 1, can be now evaluated from Eqs. (12a) and (12b) in terms of the $\mathbf{M}_{AS}^{\pm}$ matrix elements [Eq. (15)]

$$r_{ALS}^{\pm} = \frac{(M_{AS}^{\pm})_{21}}{(M_{AS}^{\pm})_{11}} = \frac{r_{AL}^{\pm} + r_{LS}^{\pm} \Psi_{AL}^{\pm} e^{-2i\gamma N_L^{\pm} t_L}}{1 - r_{LA}^{\pm} r_{LS}^{\pm} e^{-2i\gamma N_L^{\pm} t_L}} , \tag{18}$$

$$\mathbf{t}_{ALS}^{\pm} = \frac{1}{(M_{AS}^{\pm})_{11}} = \frac{\mathbf{t}_{AL}^{\pm} \mathbf{t}_{LS}^{\pm} e^{-i\gamma N_L^{\pm} t_L}}{1 - r_{LA}^{\pm} r_{LS}^{\pm} e^{-2i\gamma N_L^{\pm} t_L}} . \tag{19}$$

These reflection and transmission coefficients can be, in principle, successfully used for the evaluation of the CPKE and the CFE from Eqs. (7) and (8), respectively. As it has been discussed earlier, we can deduce the general expressions for the CPKE and the CFE from Eqs. (10) supposing that only the layer L is magnetically active. The optical reflectivity and transmission which enter these equations are calculated for the layered structure supposing that all the layers are nonmagnetic, omitting the $\pm$ superscripts in Eqs. (11)–(19). Note that when the layer L is separated from the isotropic half-spaces A and S by single interfaces, Eqs. (18) and (19) reduce to the well-known expressions for ordinary reflectivity and transmission of a single layer.[35]

2. *General expression of the polar Kerr effect*

To obtain the general analytical expression for the CPKE of the layered structure represented in Fig. 1, the reflection coefficient of the equivalent system, expressed by Eq. (18) without the $\pm$ superscripts, has to be introduced into Eq. (10a). In our case, when only the layer L is magnetically active,

$$\Phi_K^{(ALS)} = -i \frac{\partial r_{ALS}}{\partial N_L} \frac{\Delta N_L}{r_{ALS}} . \tag{20}$$

When calculating the derivative of the reflection coefficient one must bear in mind that all the reflection

and transmission coefficients of the generalized interfaces appearing in Eq. (18) depend on the complex refractive index N_L, because they are rational functions of the Fresnel reflection and transmission coefficients at the interfaces between the layer L and the neighboring layers $k-1$ and $k+1$ (Fig. 1). The general expression of the CPKE in the layered structure containing one magnetic layer writes

$$\Phi_K^{(ALS)}(r_{AL},r_{LA},r_{LS},\mathbf{t}_{AL}\mathbf{t}_{LA},\Psi_{AL},L)=\frac{\Delta N_L}{2N_L}\mathbf{t}_{AL}\mathbf{t}_{LA}\frac{4\gamma N_L t_L r_{LS}e^{-2i\gamma N_L t_L}+i(1+r_{LS}^2e^{-2i\gamma N_L t_L})(e^{-2i\gamma N_L t_L}-1)}{(1-r_{LA}r_{LS}e^{-2i\gamma N_L t_L})(r_{AL}+r_{LS}\Psi_{AL}e^{-2i\gamma N_L t_L})} . \quad (21)$$

The terms in the brackets of $\Phi_K^{(ALS)}$ stand here for the relevant general parameters of the sandwiching structures. In the ultrathin film limit approximation applied to the magnetic layer L, when only the lowest order term of the Taylor polynomial of the CPKE in t_L is considered, the exact Eq. (21) simplifies to

$$\Phi_K^{(ALS)}(r_{AL},r_{LA},r_{LS},\mathbf{t}_{AL}\mathbf{t}_{LA},\Psi_{AL},L)\approx\frac{\mathbf{t}_{AL}\mathbf{t}_{LA}\Delta N_L\gamma t_L(1+r_{LS})^2}{(1-r_{LA}r_{LS})(r_{AL}+r_{LS}\Psi_{AL})} . \quad (22)$$

3. *General expression of the Faraday effect*

To derive the general expression of the CFE exhibited by the layered system represented by the structure shown in Fig. 1, we used the same procedure as for the CPKE. The transmission coefficient, expressed by Eq. (19) without the $\pm$ superscripts, enters equation (10b), which for only one magnetic layer simplifies to

$$\Phi_F^{(ALS)}=i\frac{\partial \mathbf{t}_{ALS}}{\partial N_L}\frac{\Delta N_L}{\mathbf{t}_{ALS}} . \quad (23)$$

After some algebra one obtains the CFE general expression

$$\Phi_F^{(ALS)}(r_{LA},r_{LS},L)=\frac{\Delta N_L}{2N_L}\frac{2\gamma N_L t_L(1+r_{LA}r_{LS}e^{-2i\gamma N_L t_L})+i(e^{-2i\gamma N_L t_L}-1)(r_{LA}+r_{LS})}{1-r_{LA}r_{LS}e^{-2i\gamma N_L t_L}} . \quad (24)$$

We would like to emphasize that Eq. (24) is symmetric with the respect to the reflection coefficients r_{LA} and r_{LS}, which confirms the fact that the transmitted wave comes from a single pass propagation through the layer L or is reflected at both effective interfaces. When the magnetic layer becomes ultrathin, Eq. (24) simplifies to

$$\Phi_F^{(ALS)}(r_{LA},r_{LS},L)\approx\gamma\Delta N_L t_L\frac{(1+r_{LA})(1+r_{LS})}{1-r_{LA}r_{LS}} . \quad (25)$$

4. *Generalized formulas for a magnetic multilayer*

Thanks to the linear superposition principle [Eqs. (10)], the MO response of a magnetic multilayer is expressed as a sum of the MO contributions of all magnetic layers. Each contribution corresponds to the case of a structure where only one layer is magnetized, as treated by our method. To derive the general formulas for a particular structure the matrices (16) and (17) have to be calculated. The matrix elements lead directly to the reflection and transmission coefficients of the effective interfaces [Eqs. (12)] and also to Ψ_{AL} [Eq. (14)]. When these coefficients are introduced into the general formulas, the analytical expressions for the MO contribution of a specific layer are obtained.

This procedure is very efficient, especially for systems containing more layers. At the same time the accuracy of these expressions is practically equal to that of the full matrix calculation, because for the first-order MO effects (linear in magnetization) only the approximation of small ellipsometric angles is employed.

C. Analytical expressions of MO effects in simple film structures

1. *Polar Kerr effect*

Now we will apply the general expression (21) to the simple layered structures considered in Table I. Starting from the system $K1$ of an ultrathin magnetic layer deposited on a thick buffer (studied generally by *in situ* measurements) and arriving at the sandwich structure $K3$ grown on a thick substrate (studied mainly *ex situ)* we will show, how each individual layer added to the system changes its MO response.

In each system the reflection and transmission coefficients of the effective interfaces should be evaluated. For example, for the system $K1$ we have $r_{AL}=-r_{LA}=r_{02}, r_{LS}=r_{21}$, $\mathbf{t}_{AL}\mathbf{t}_{LA}=1-r_{02}^2$, and $\Psi=1$, where r_{02} and r_{21} are defined by Eq. (4a). The deduced expressions describe exactly the MO interaction of the light within a given structure. However, they are quite complicated to be physically understood. Within the ultrathin-magnetic-film approximation these expressions are simplified.

The simplification of the formulas (Table I) is possible

TABLE I. Analytical expressions of the complex polar Kerr effect in simple structures. The ultrathin-magnetic-film approximation was used.

Identification	Structure	Thickness	Isotropic refractive index	Approximate expression of the CPKE
	Ambient	∞	N_0	
$K1$	Magnetic layer	t_2	N_2	$\Phi_K^{(02\underline{1}1)} \approx 4\gamma \Delta N_2 t_2 N_0 N_2 (N_0^2 - N_1^2)^{-1}$
	Nonmagn thick buffer	∞	N_1	
	Ambient	∞	N_0	
	Nonmagn overlayer	t_1	N_1	
$K2$	Magnetic layer	t_2	N_2	$\Phi_K^{(01\underline{2}1)} \approx \Phi_K^{(02\underline{1}1)} e^{-2i\gamma N_1 t_1}$
	Nonmagn thick buffer	∞	N_1	
	Ambient	∞	N_0	
	Nonmagn overlayer	t_1	N_1	
$K3$	Magnetic layer	t_2	N_2	$\Phi_K^{(01\underline{2}14)} \approx \Phi_K^{(02\underline{1}1)} \Phi_{KC} e^{-2i\gamma N_1 t_1}$
	Nonmagn buffer layer	t_3	N_1	
	Float glass substrate	∞	N_4	[for Φ_{KC} see Eq. (26)]

in the present approximation because the magnetic film is "optically neglected" in the structure; only its MO activity is taken into account. In other words this means, that the thickness of the magnetic layer is supposed to be small enough to avoid any perturbation of the optical properties (reflectivity or transmission) of the system. As we will show later from numerical calculations, the perturbation introduced by the metallic layers is sometimes not negligible, even for ultrathin layers ($t \sim 1$ nm). Although the departure from the rigorous theory (i.e., exact expressions or the matrix models) is not very important, the simplified expressions obtained using the ultrathin-magnetic-film limit cannot be successfully employed for the *precise* evaluation of the MO effects. However, the *simplification* of the formulas is *significant* as it makes them suitable to explain the trends in the MO response of the structure. Since the optical perturbation of the system introduced by the magnetic layer is neglected, the CPKE is then proportional to its thickness.

Let us now focus on the simplified expressions displayed in Table I. Since N_2 and ΔN_2 vary rather slowly with the photon energy,[32] the variation of the CPKE in the system $K1$ comes mainly from the term $(N_0^2 - N_1^2)^{-1}$. The expression can be also rewritten in another form, the $\Phi_K^{(02\underline{1}1)}$ being proportional to the term $t_{01} t_{10} r_{01}^{-1}$, as a function of the reflection and transmission coefficients at the *ambient-buffer* interface. So, one can see that the CPKE spectral shape is very sensitive to the optical properties of the buffer layer.

When an overlayer is added, with the same optical properties as the buffer layer (structure $K2$), the new CPKE $\Phi_K^{(01\underline{2}1)}$ is equal to $\Phi_K^{(02\underline{1}1)}$ multiplied only by an exponential attenuation factor, because there is no other "available" interface in the structure which could reflect the light and produce some interference phenomena, in the considered approximation.

When the buffer layer thickness is limited (structure $K3$), such "available" interface appears, and the waves propagating through the buffer layer are partly reflected backward. To account for this effect $\Phi_K^{(01\underline{2}1)}$ has to be multiplied by the correction factor Φ_{KC}

$$\Phi_{KC} = \frac{r_{01}(1 + r_{14} e^{-2i\gamma N_1 t_3})^2}{(1 + r_{01} r_{14} e^{-2i\gamma N_1 (t_1 + t_3)})} \times \frac{1}{(r_{01} + r_{14} e^{-2i\gamma N_1 (t_1 + t_3)})} . \quad (26)$$

This term takes into account the total thickness of nonmagnetic layers $t_1 + t_3$ [see denominator of Eq. (26)] and also the buffer layer thickness which specifies the position of the magnetic layer in a whole nonmagnetic film. As expected, $\Phi_{KC} \to 1$ when $t_3 \to \infty$.

2. *Faraday effect*

For the calculation of the MO response in light transmission two structures, $F1$ and $F2$ (Table II) are considered. Analytical expressions of the CFE are obtained from the general one [Eq. (24)]. For example, in the structure $F1$ we have $r_{LA} = r_{LS} = r_{20}$.

Within the ultrathin-magnetic-film approximation the expressions are again simplified. As demonstrated in Table II, the presence of the sandwich layers is, in this approximation, accounted by the correction factor Φ_{FC}

$$\Phi_{FC} = \frac{N_0 (1 - r_{01} e^{-2i\gamma N_1 t_1})(1 - r_{01} e^{-2i\gamma N_1 t_3})}{N_1 (1 - r_{01}^2 e^{-2i\gamma N_1 (t_1 + t_3)})} . \quad (27)$$

The particular cases, when only one of the sandwich layers is present ($t_1 = 0$ or $t_3 = 0$), are also included. As expected, $\Phi_{FC} = 1$ when $t_1 = t_3 = 0$.

D. Transparent substrate effects

Up to now we considered structures without transparent substrate in Faraday configuration (structure $F2$ in Table II) or deposited on a semi-infinite medium in Kerr configuration (structure $K3$ in Table I) which is quite a good compromise between the accuracy of the model and

TABLE II. Analytical expressions of the complex Faraday effect in simple structures. The ultrathin-magnetic-film approximation was used.

Identification	Structure	Thickness	Isotropic refractive index	Approximate expression of the CFE
	Ambient	∞	N_0	
$F1$	Magnetic layer	t_2	N_2	$\Phi_F^{(020)} \approx \gamma \Delta N_2 t_2 N_2 N_0^{-1}$
	Ambient	∞	N_0	
	Ambient	∞	N_0	
	Nonmagnet overlayer	t_1	N_1	
$F2$	Magnetic layer	t_2	N_2	$\Phi_F^{(01\bar{2}10)} \approx \Phi_F^{(020)} \Phi_{FC}$
	Nonmagnet buffer layer	t_3	N_1	
	Ambient	∞	N_0	[for Φ_{FC} see Eq. (27)]

its simplicity. Optical (reflection of the light at the free substrate interface and its secondary interaction with the magnetic system) and magneto-optical (Faraday rotation) contributions of the substrate (usually float glass) have to be considered now.

If the MO activity of the real substrate can be neglected, the approximation of the semi-infinite transparent substrate medium gives in the Kerr configuration usually *good results.* In Faraday configuration the approximation is not so good because the presence of the substrate is not considered. When evaluating the MO response of the sample grown on a thick transparent substrate we must take into account that the coherence length for the quasimonochromatic light employed in the spectroscopic experiments is much smaller than the thickness of our float glass substrate.

To evaluate the CFE in the glass substrate alone, with thickness t_G and circular birefringence ΔN_G, one can use an approach[37] based on Stokes vectors and Mueller matrices[35]

$$\Phi_{FG} \approx \frac{1+R_G^2 A_G^2}{1-R_G^2 A_G^2} \Delta N_G \gamma t_G \ . \tag{28}$$

Here $\Delta N_G \gamma t_G$ is the CFE in bulk glass, $R_G = |(N_G-1)/(N_G+1)|^2$, and $A_G = \exp(-2\gamma |\mathcal{F}(N_G)| t_G)$.

In the case of the real sample we need to describe the interaction of partially coherent light with an optically anisotropic stratified medium. For metallic layer structures deposited on thick transparent dielectric substrates we found very efficient to use a procedure based on a beam summation technique. In this approach the light interaction in the layered structure deposited on the thick substrate is supposed to be coherent and thus it can be described in terms of Yeh's matrix formalism. On the other hand, the optical interaction in the thick transparent substrate is supposed to be noncoherent.

In our calculation, which is quite similar to that carried out in Sec. I B, we will keep the notation defined in Fig. 1, but now the substrate corresponds to L, ambient media are identified as A and S and the layered structure deposited on the transparent substrate is described by an effective interface between the A and L media. The effective interface is characterized by the reflection and transmission coefficients for RCP and LCP waves which are obtained from Eqs. (12), with matrices $\mathbf{M}^+$ and $\mathbf{M}^-$ given by Eq. (3).

Let us suppose that the incident beam is a superposition of RCP and LCP waves with the same field amplitudes. Multiple reflections occur in the transparent substrate. Consider the phase factors for RCP (+) an LCP (−) waves in the substrate

$$\varphi_\pm = \gamma t_G [n_G \pm \Delta n_G - i(k_G \pm \Delta k_G)] \ . \tag{29}$$

The series used for calculation of the reflection coefficients of RCP and LCP waves

$$r^\pm = r_{AL}^\pm + e^{-2i\varphi_\pm} \mathbf{t}_{AL}^\pm \mathbf{t}_{LA}^\pm r_{LS}^\pm (1 + r_{LA}^\pm r_{LS}^\pm e^{-2i\varphi_\pm} + \cdots)$$

$$= \sum_{i=0}^{\infty} \rho_i^\pm \ , \tag{30}$$

are then transformed, converting the terms ρ_i^+ and ρ_i^- to Stokes vectors[35] $\mathbf{s}_i$

$$s_{i,0} = \tfrac{1}{2}(|\rho_i^+|^2 + |\rho_i^-|^2) \ , \tag{31a}$$

$$s_{i,1} = s_{i,0} \cos(2\epsilon_{Ki}) \cos(2\theta_{Ki}) \ , \tag{31b}$$

$$s_{i,2} = s_{i,0} \cos(2\epsilon_{Ki}) \sin(2\theta_{Ki}) \ , \tag{31c}$$

$$s_{i,3} = s_{i,0} \sin(2\epsilon_{Ki}) \ , \tag{31d}$$

where θ_{Ki} and ϵ_{Ki} are calculated from the terms ρ_i^+ and ρ_i^- using Eqs. (7a) and (7b). The procedure allows us to maintain the phase relation between RCP and LCP waves of the same reflection order i at the free substrate side, while the interaction between the waves at different reflection orders in the transparent substrate can be supposed to be noncoherent. This noncoherent superposition is represented by the series of Stokes vectors

$$\mathbf{S} = \sum_{i=0}^{\infty} \mathbf{s}_i \ . \tag{32}$$

The convergence of Eq. (32) is usually very fast. For a qualitative explanation of the glass substrate effects it is sufficient to take the first two terms only. In our calculations we used $i \leq 10$.

From the resulting Stokes vector $\mathbf{S}$ given by Eq. (32),

the reflection optical characteristics of the structure, i.e., reflectivity $R=S_0$, polar Kerr rotation θ_K, and ellipticity ϵ_K, can be evaluated

$$\theta_K=\frac{1}{2}\arctan\frac{S_2}{S_1}\ , \tag{33a}$$

$$\epsilon_K=\frac{1}{2}\arctan\frac{S_3}{\sqrt{S_1^2+S_2^2}}\ . \tag{33b}$$

The same procedure applied to transmitted beams provides the transmission, Faraday rotation and ellipticity quantities.

II. SAMPLES, EXPERIMENTAL DETAILS, AND DATA ANALYSIS

A. Sample preparation and characterization

The preparation of Au/Co/Au samples and the characterization of their structure and texture by grazing angle x-ray reflectometry, electron diffraction, scanning tunneling microscopy, transmission electron microscopy, reflection high-energy electron diffraction and soft x-ray reflectometry were reported earlier.[38–43] We will summarize below the important features.

The Au/Co/Au ultrathin film structures were prepared by thermal evaporation of the metals (Au buffer: 0.2 nm/s, Co layer: 0.005 nm/s, Au overlayer: 0.05 nm/s) in ultrahigh vacuum ($p\approx10^{-10}$ Torr) on cleaned 1 mm thick float glass substrates. The first Au buffer layer, 25 nm thick, was annealed at 175 °C to reduce the surface roughness. In this way an Au[111] textured fcc polycrystalline film is obtained, with an average lateral crystallite size of about 100 nm. The Au buffer layer surface consists of terraces with an average lateral size of 30 nm, limited by monoatomic steps.[39] The buffer layer thickness of 25 nm is necessary to avoid holes and to obtain a surface roughness of 0.5 nm.[40,42] The cobalt is deposited afterwards at room temperature. It shows a polycrystalline hcp structure with (0001) planes parallel to the film surface.[41] In the considered Co thickness range, between 2 and 10 atomic layers (one atomic layer corresponds here to 0.203 nm), the Co crystalline structure and roughness (0.5 nm) are preserved.[40] Finally, it is usually covered by a 5 nm thick Au protective overlayer without further annealing. Other samples were prepared with different overlayer thicknesses to check its influence on the magnitude of MO effects. The layer thickness was monitored by a quartz oscillator first calibrated using grazing angle x-ray reflectivity. The presence of abrupt interfaces between Au and Co layers was confirmed by cross-section electron microscopy.[42,43] The sandwich structure is sufficiently thin to enable optical measurements in light transmission.[20]

The studies of Au layers and float glass substrate contribution, both to MO reflection and transmission spectra, were performed separately on Au films prepared by *e*-beam evaporation, their thicknesses range from 40 to 190 nm. An accurate study of the Co thickness dependence of magneto-optical effects has been carried out on a Co stepped wedge sample.[27]

B. Magneto-optical experiments

Room-temperature magneto-optical polar Kerr and Faraday effect experiments were performed on a MO spectrometer working in the 1.5–5.2 eV spectral region with an accuracy of 10^{-4} deg. The azimuth modulation technique, where the magneto-optical effect of the sample is compensated by Faraday rotation in a fused quartz rod, was employed.[44] The optical sequence of the spectrometer consists of Xe arc lamp, prism monochromator, polarizer, Faraday effect compensation and modulation cells, sample, analyzer, and photomultiplier. To extract the ellipticity signal, a pair of calibrated phase plates is inserted between the modulation cell and the sample. All stray effects, including Faraday rotation in the air between electromagnet pole pieces, were compensated. The polarized quasimonochromatic light beam ($\Delta E\sim0.02$ eV) penetrated the sample from the film side. In the polar Kerr effect configuration the angle of incidence was small (5 deg). The available magnetic fields in Kerr (Faraday) measurements were 1.4 T (0.25 T) but 0.18 T was already sufficient to saturate the magnetization of the samples in the direction perpendicular to the film plane.

C. Theoretical procedures and optical constants used for calculations

To explain the MO data in Au/Co/Au/ *float glass* thin-film structures we use the models of optical interactions within magnetic layered structures described in Sec. I. Firstly, for the comparison between an exact theory and our experimental data, and secondly, for a numerical simulation of the MO spectra variation with layer

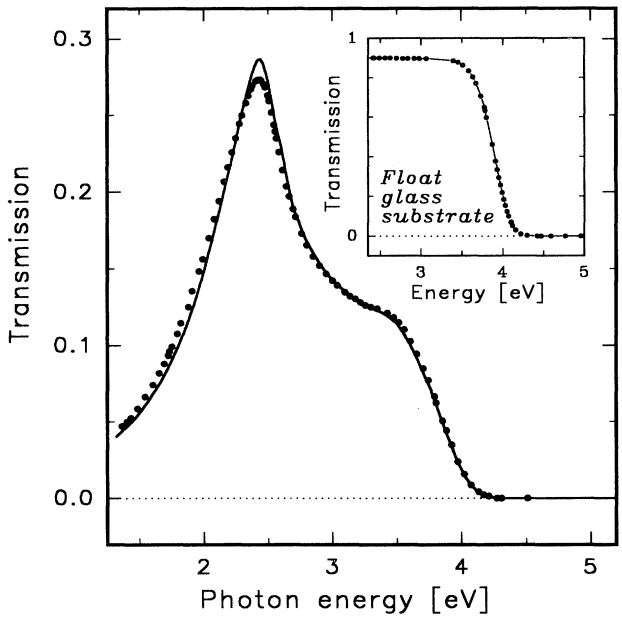

FIG. 2. Experimental transmission curve of the Au (5 nm)/Co (0.95 nm)/Au (25 nm)/ *float glass* (1 mm) sandwich structure (black dots) compared with the result of a calculation based on the matrix model (solid line). The inset shows details of the absorption edge of the float glass substrate.

thicknesses, a full matrix model based on Yeh's formalism (Sec. I A) is employed, including noncoherent interactions in the float glass substrate (Sec. I D). The observed trends are then explained in terms of the simplified analytical expressions of MO effects, deduced in Sec. I B and displayed in Tables I and II.

In all our calculations we suppose that the interfaces between neighboring layers are extremely sharp and the layers are optically homogeneous, i.e., the structure can be modeled considering a steplike optical profile. Since the optical data related to our ultrathin metallic films are not available, we use the data pertaining to bulk metals.

The choice of the optical and magneto-optical data for modeling the optical interactions in Au/Co structures was discussed recently.[32] The employed optical constants for Au are the same as these reported in Ref. 32. For Co layers we use optical data of Johnson and Christy[45] determined for samples prepared by evaporation on fused quartz substrates. Magneto-optical data for Co were calculated[32] from complex polar Kerr effect spectra[46] measured at near normal incidence on a 110 nm thick Co film prepared by *e*-beam evaporation. The off-diagonal tensor elements, derived from recent polar Kerr effect spectra of Co, reported by Brändle *et al.*,[47] give similar results.

For a more precise evaluation of the optical interactions in our samples, and especially for calculation of glass substrate effects, optical and magneto-optical characteristics of our float glass substrates are needed.

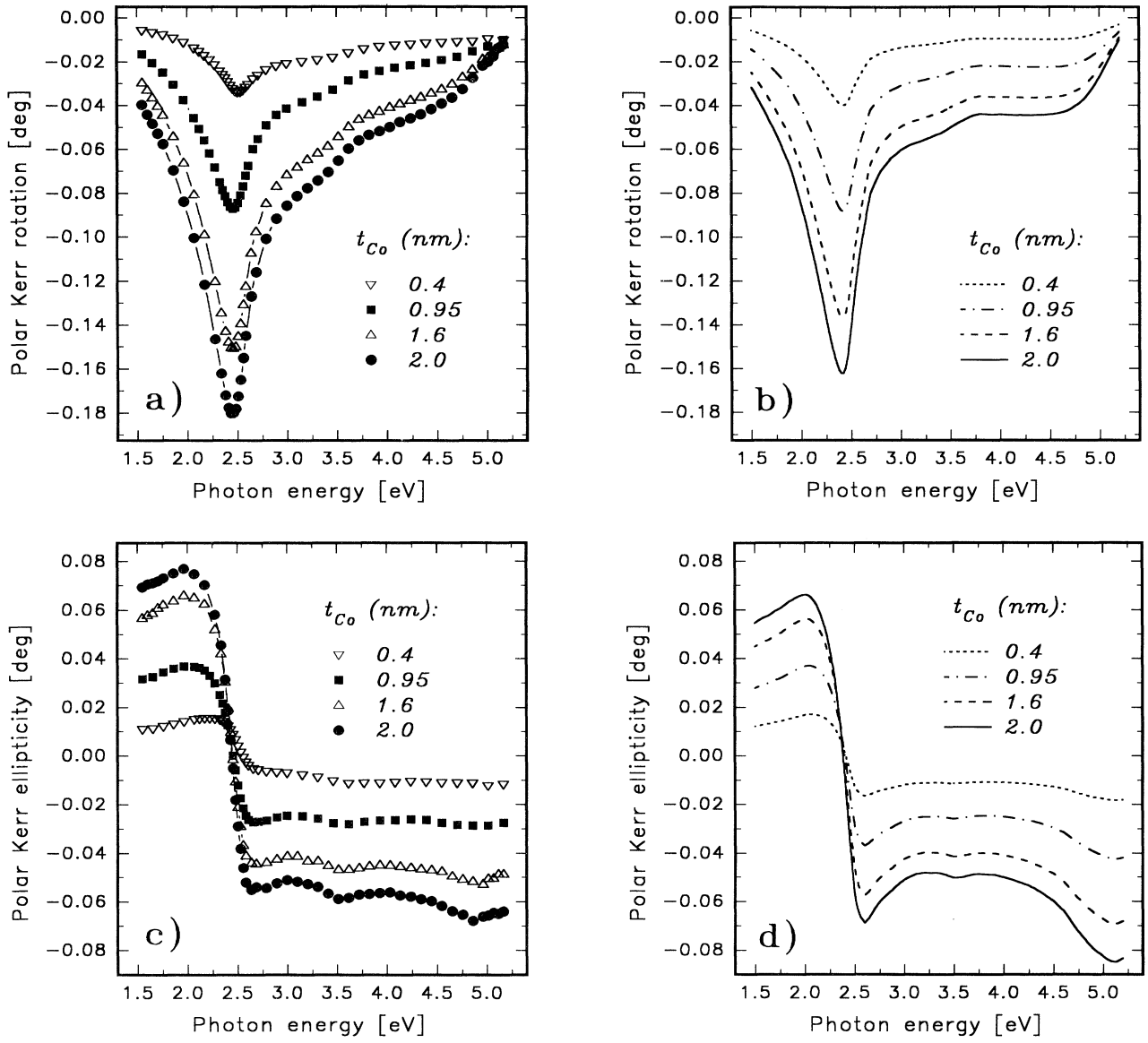

FIG. 3. Saturated MO polar Kerr rotation spectra: (a) experiment, (b) matrix calculation results, and polar Kerr ellipticity spectra: (c) experiment, (d) matrix calculation results, in the Au (5 nm)/Co (t_{Co})/Au (25 nm)/ *float glass* (1 mm) samples for different values of t_{Co}.

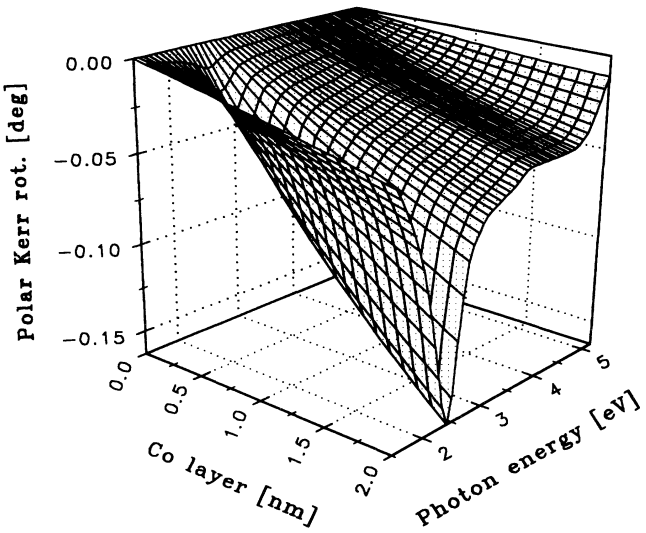

FIG. 4. Variation of the polar Kerr rotation spectrum with the Co layer thickness in the Au (5 nm)/Co (t_{Co})/Au (25 nm)/ *float glass* (1 mm) structure. Matrix model.

For this purpose we carried out several spectroscopic experiments which provided Faraday rotation and ellipticity, refractive index (using Brewster angle measurements) and extinction coefficient (obtained from transmission spectra).

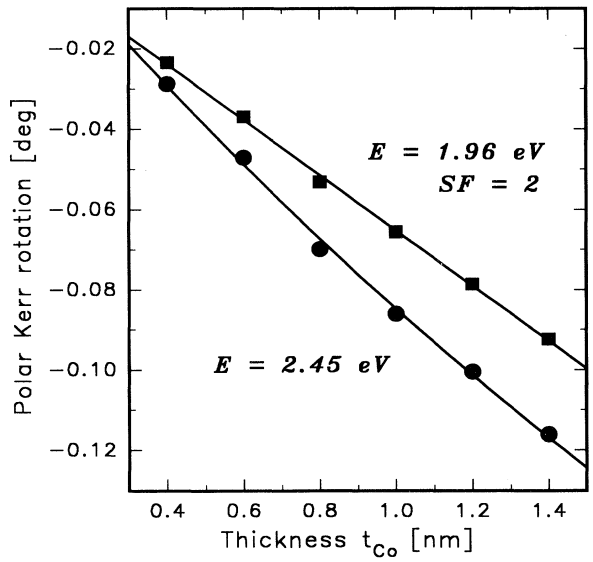

FIG. 5. Variation of the polar Kerr rotation with the Co layer thickness in the Co stepped wedge Au (5 nm)/Co (t_{Co})/Au (25 nm)/ *float glass* (1 mm) sample at photon energies of 2.45 and 1.96 eV: experimental (symbols) and adjusted theoretical curves. The values of 1.96 eV were multiplied by a scaling factor $SF=2$. Error bars are smaller than the symbol size.

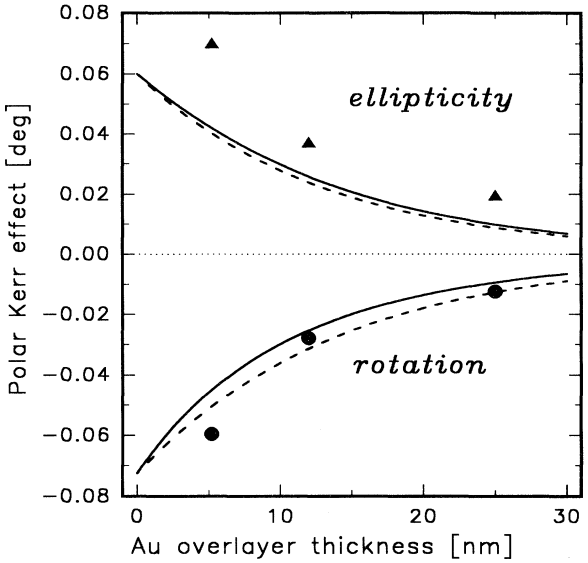

FIG. 6. Variation of the complex polar Kerr effect, measured at 1.96 eV, with the Au overlayer thickness in the Au (t_1)/Co (1.15 nm)/Au (25 nm)/ *float glass* (1 mm) structure. The experimental values of polar Kerr rotation (circles) and polar Kerr ellipticity (triangles) are compared with the matrix calculation (solid lines) and with an exponential dependence on Au overlayer thickness (dashed lines).

III. DISCUSSION OF THEORETICAL AND EXPERIMENTAL RESULTS IN Au/Co/Au FILMS

In this part we will show how the experimental MO data can be analyzed using the analytical expressions (Tables I and II). They have been deduced from the general exact formulas and simplified by the ultrathin magnetic layer approximation. Calculations based on these simplified expressions will be compared with the experi-

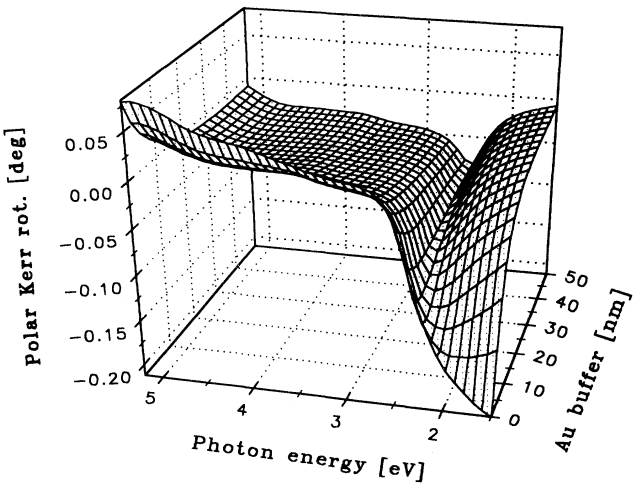

FIG. 7. Variation of the polar Kerr rotation with the Au buffer layer thickness in the Au (5 nm)/Co (1 nm)/Au (t_3)/ *float glass* (1 mm) structure. Matrix model.

mental data and with the results of the exact calculations. Firstly, this comparison will show the validity of the approximation employed. Secondly, it will check the approximation, acceptable from the point of view both of the accuracy and the simplicity. We will begin our discussion of the experimental MO data for Au/Co/Au sandwich structures with the analysis of the MO effect provided by the Co layer itself, and after we will look at the effects of the glass substrate and to weak[48] MO effects due to Au layers.

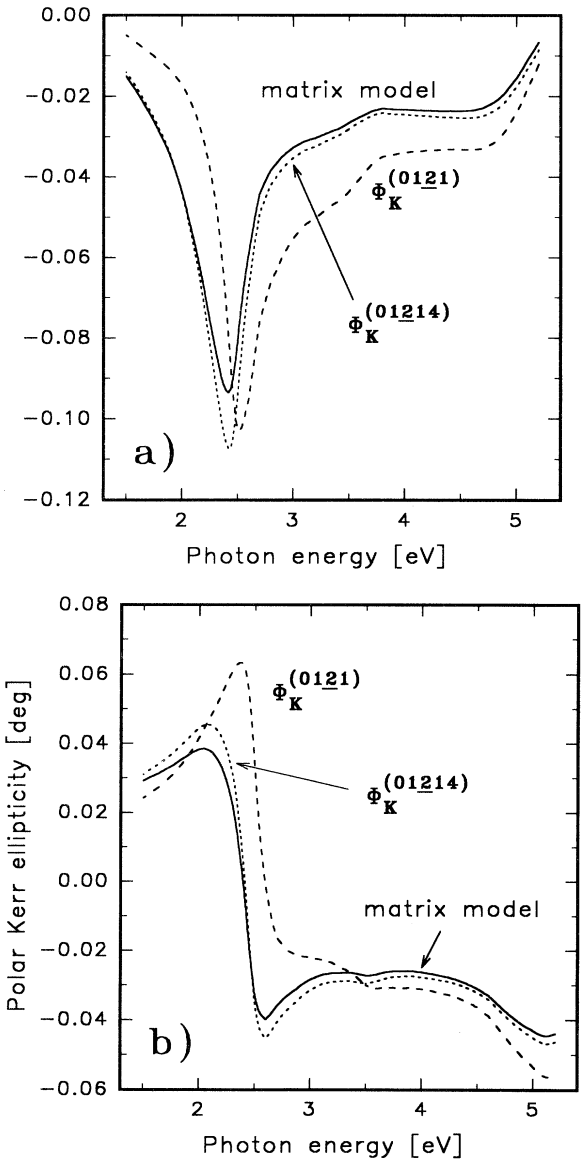

FIG. 8. Theoretical polar Kerr rotation (a) and Kerr ellipticity (b) spectra calculated by the matrix model (solid lines) for the Au (5 nm)/Co (1 nm)/Au (25 nm)/ *float glass* (1 mm) structure and using the simplified expressions within an ultrathin-magnetic-film approximation (see Table I), for an overlayered MO layer on a thick Au buffer (dashed line) and with the correction due to a finite Au buffer layer thickness (short dashes).

A. Light transmission

The typical transmission spectrum of the Au/Co/Au sandwich deposited on float glass is shown in Fig. 2 for $t_{Co}=0.95$ nm; it is well explained by our model, which is also able to reproduce the t_{Co} variation of the transmission curves. Its shape is similar to the transmission curve of a 40 nm thick Au film. The maximum transmission at 2.45 eV reflects the plasma edge behavior in gold near this energy, where the absorption edge of the interband transitions takes place. This behavior is clearly revealed[32] in the spectrum of the imaginary part of the Au permittivity. The structure displayed around 3.5 eV is also due to Au.[32] At 4.2 eV the sample is no longer transparent because of a strong light absorption in the glass substrate (see inset in Fig. 2). This reduces the spectral region covered by Faraday effect measurements.

B. Polar Kerr effect

Figure 3 compares experimental spectra of (a) polar Kerr rotation (PKR) and (c) polar Kerr ellipticity (PKE) for perpendicularly magnetized samples at saturation with full calculations (b) and (d), for several Co thicknesses lying between 0.4 and 2.0 nm. We observe well a typical shape of the spectra near 2.45 eV induced by the optical behavior of Au near the plasma edge, a negative peak in PKR and a corresponding steep change in the sign of PKE. This behavior is observed in all the samples studied here and it should be pointed out that the geometry and the quality of our samples allow to evidence a sharper structure than in the corresponding multilayers.[49–52] Moreover, the structure at 3.5 eV, originating from Au, also appears in PKR as in the transmission spectrum. As expected, the magnitude of the MO effects increases with t_{Co}. This dependence will be discussed below in more detail. Such MO polar Kerr effect spectra are well explained by electromagnetic theory.[32,33] The differences between experimental and calculated amplitudes, as well as small differences in the spectral shape which are observable in PKE at 2.7 and 5 eV, could be explained by the fact that the employed optical parameters somewhat differ from these, displayed by our layers.

As it has been shown in Table I, in the ultrathin Co film approximation, the CPKE in the studied samples can be expressed by a product of three terms: the correction factor Φ_{KC} for finite buffer layer thickness, the exponential attenuation term coming from the overlayer, and $\Phi_K^{(02\underline{1})}$. The last, most important term represents the CPKE in a thin Co film deposited on a semi-infinite Au buffer, which in our case ($N_0=1$) simplifies to

$$\Phi_K^{(02\underline{1})} \approx \frac{4\gamma N_{Co}\Delta N_{Co} t_{Co}}{1-N_{Au}^2} . \tag{34}$$

This relation reflects the following essential features: (a) the linear dependence of the CPKE on the complex circular birefringence ΔN_{Co}, as expressed from Eq. (20); (b) the linear dependence on the Co layer thickness t_{Co}, resulting from the ultrathin film approximation, and (c) the large spectral anomalies in the Au plasma edge region, where $n_{Au}=\mathcal{R}(N_{Au})\simeq 1$, carried by the denominator of

Eq. (34). Note that a thick enough Au buffer is essential to provide a large spectral anomaly, consistently with the expectation for the Φ_{KC} expression [Eq. (26)].

We can then suppose that the shape of the CPKE spectra will not depend very much on the Co thickness. This was confirmed both by our experimental results (Fig. 3) and by the modeling of the Co thickness dependence of the CPKE, using the matrix formalism. The result of modeling the PKR dispersion as a function of t_{Co} is displayed in Fig. 4, where only a very small shift (0.018 eV) of the peak position to lower photon energies takes place when increasing the Co layer thickness from 0 to 2 nm. At the same time a small departure from the linearity in the Co thickness dependence can be observed, detected in the plasma edge region (Fig. 5).

The effect of the Au overlayer can be approximately represented by the exponential factor $e^{-2i\gamma\tilde{N}_1 t_1}$ (Table I). The dependence of the CPKE on the Au overlayer thickness, predicted by the exact formula, is of course more complicated. However, in our case, the deviation from a pure exponential variation in the vicinity of the Au plasma edge is rather small. Even at 1.96 eV the exponential variation with the Au overlayer thickness agrees reasonably well with theoretical predictions, as demonstrated in Fig. 6.

Consistently with the formulas of Table I the shape of the CPKE dispersion spectra is not strongly affected by the variation of the Au overlayer thickness. For exam-

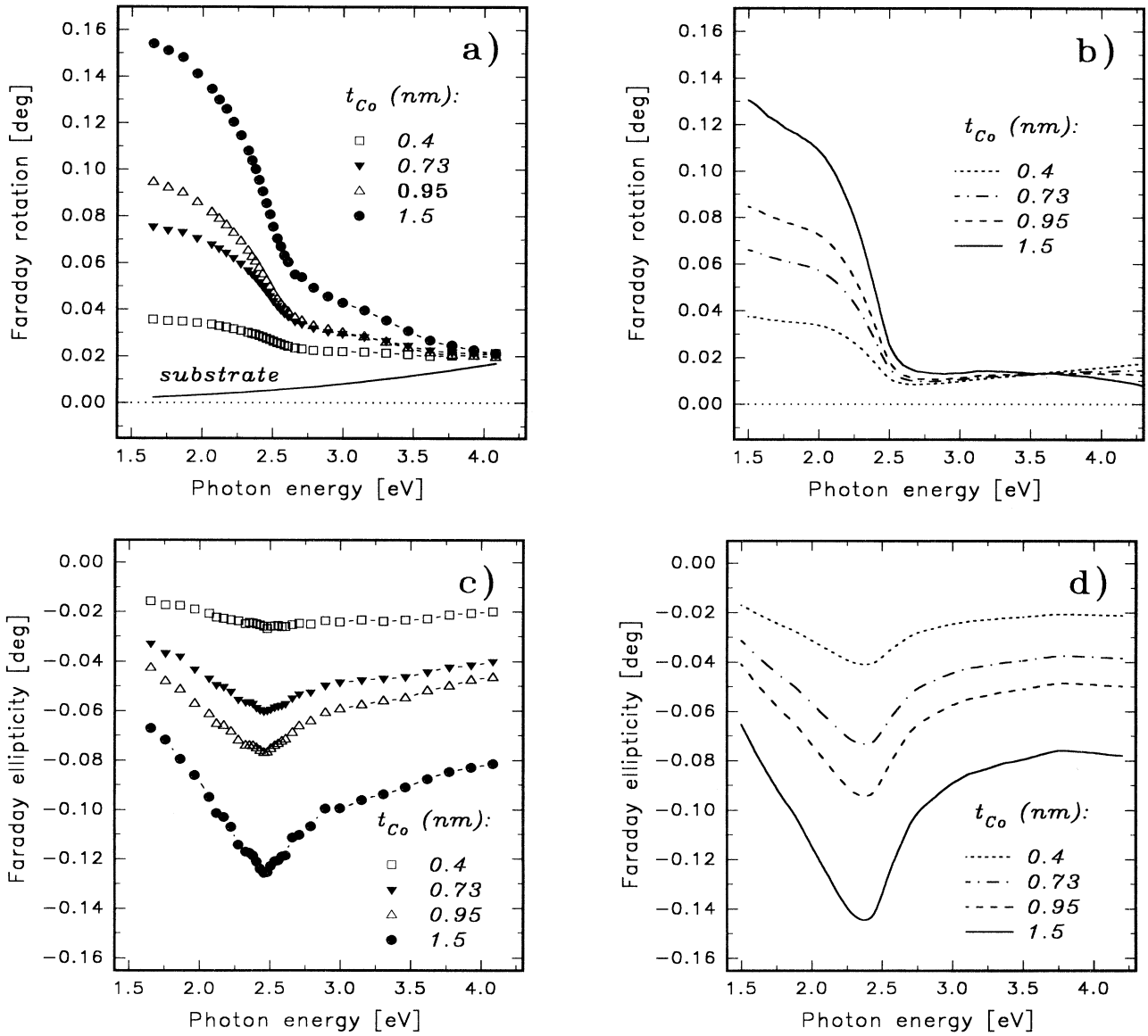

FIG. 9. Saturated Faraday rotation spectra (a) experiment, (b) matrix calculation, and Faraday ellipticity spectra (c) experiment, (d) matrix calculation, in Au (5 nm)/Co (t_{Co})/Au (25 nm)/ *float glass* (1 mm) structures. The measurements were performed in a remanent field of 0.01 T (for details see text), the contribution of the float glass substrate to the Faraday rotation is shown in (a).

ple, the peak position in the PKR spectrum changes only by 0.02 eV when varying the overlayer thickness between 0 and 10 nm.

On the contrary, significant changes of the CPKE spectra are expected (Table I) when varying the Au buffer thickness. When it is reduced, the reflection at the interface between the Au buffer layer and the glass substrate starts to play a more significant role. This effect strongly affects the CPKE spectra and results in the broadening and shift of the structure at 2.45 eV to lower photon energies, as exhibited in Fig. 7 for the PKR.

To check the limits of the simplified expressions, employed in the demonstration of the trends in the CPKE spectra, we compare in Fig. 8 the results of the calculation of $\Phi_K^{(01\bar{2}14)}$ and $\Phi_K^{(01\bar{2}1)}$ with those of the matrix model for a sandwich with $t_{Co}=1$ nm. One can see here that the difference between the value of $\Phi_K^{(01\bar{2}14)}$ and that calculated with the matrix model, which comes from the ultrathin-magnetic-film approximation, can be non-negligible at some photon energies, especially in the vicinity of the Au plasma edge. For example, in the PKR spectrum [Fig. 8(a)] this difference reaches 16% of the magnitude at 2.45 eV. This shows that even for ultrathin layers the conditions in which the ultrathin film approximations[29] can be successfully employed must be always carefully analyzed. On the other hand it is interesting to notice that at 1.96 eV, where both *ex situ* and *in situ* magneto-optical experiments are frequently performed, the dependence of PKR on the Co layer thickness is linear (Fig. 5).

We found that the photon energy range at which a perfect linearity with Co thickness is observed depends on the Au buffer layer thickness: for $t_3=25$ nm this happens at 1.96 eV, whereas it is 1.5 and 2.2 eV for $t_3=15$ nm and $t_3=40$ nm, respectively. Conversely, this linearity is not significantly influenced by the Au overlayer thickness.

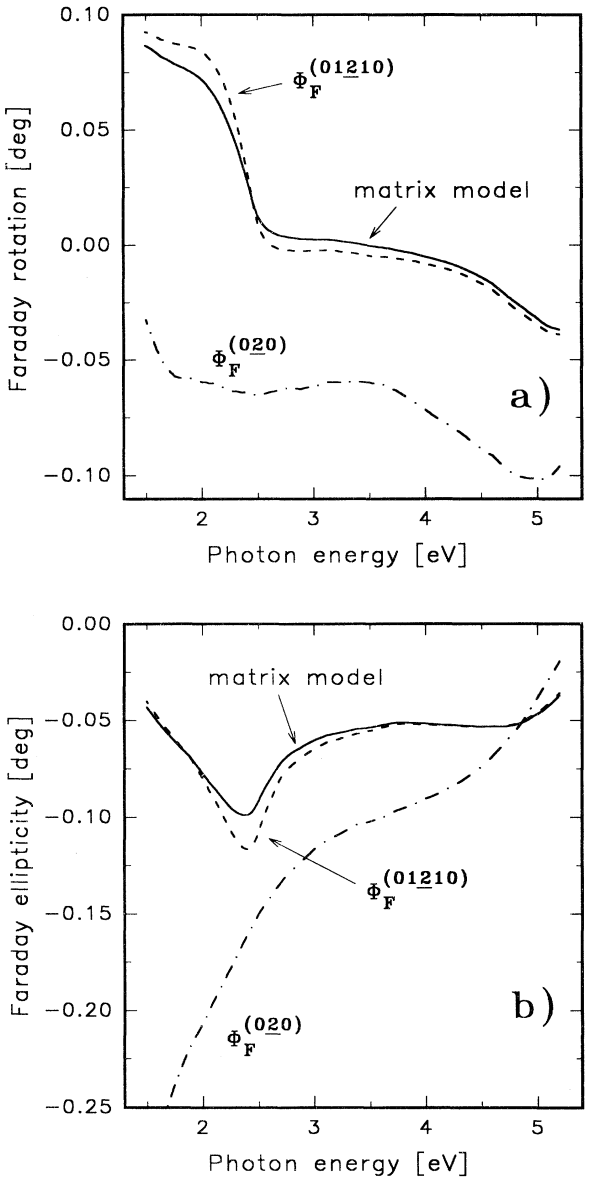

FIG. 10. Theoretical Faraday rotation (a) and Faraday ellipticity (b) spectra in the Au (5 nm)/Co (1 nm)/Au (25 nm)/ *float glass* (1 mm) structure calculated using the matrix model (solid line), compared with the calculations based on simplified expressions within the ultrathin magnetic layer approximation (see Table II): for the Au (5 nm)/Co (1 nm)/Au (25 nm) structure (dashed lines) and for a 1 nm thick free-standing Co layer (dash-dot lines).

C. Faraday effect

Both experimental and calculated complex Faraday effect spectra are collected in Fig. 9. In Faraday measurements we restricted ourselves to Co layers thinner than 1.6 nm, for which the hysteresis loops are still nearly square. That is why we were able to equate the MO signal due to the Co film obtained in the remanent field of

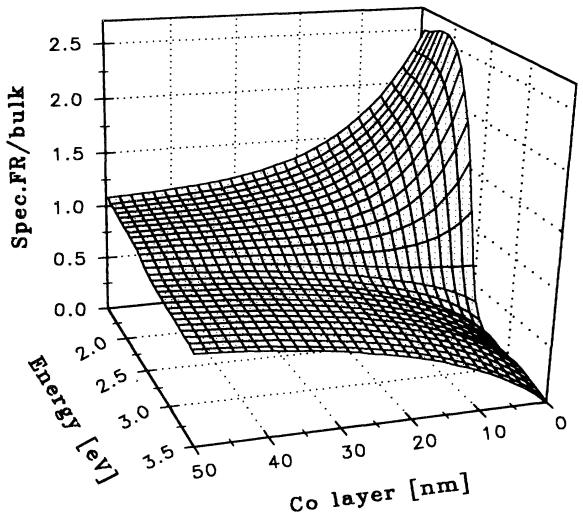

FIG. 11. Variation of the specific Faraday rotation spectrum in the Co (t_{Co})/Au (25 nm)/ *float glass* (1 mm) structure with the Co layer thickness normalized to the specific Faraday rotation in bulk Co. Matrix model.

the electromagnet with that expected for a magnetically saturated sample.

In this way the contribution of the float glass substrate to Faraday rotation (FR) was reduced to rather small values [see the solid line in Fig. 9(a)]. In the sample with $t_{Co}=1.5$ nm, where the remanent ratio was a little bit smaller than 100%, the saturation value was deduced from the field dependence of the Faraday ellipticity (FE).

In both FR [Fig. 9(a)] and FE [Fig. 9(c)] spectra we again observe a typical behavior near 2.45 eV induced by the optical properties of Au. Again as in the CPKE, there is sign of some spectroscopic Au structure around 3.5 eV. The Faraday effect increases with t_{Co}. Both FR and FE spectra are appropriately explained by the theory [Figs. 9(b) and 9(d)]; the differences in magnitudes and spectral shapes could be explained by the failure of the employed optical data to determine accurately the optical parameters of our layers.

To understand the observed spectra and the trends when changing the thicknesses of layers we can use the simplified expressions obtained in the ultrathin-magnetic-film limit without considering the glass substrate (Table II). The results of these simplified calculations are compared in Fig. 10 with the rigorous model computed for a structure deposited on a 1 mm thick glass substrate. One can see there that the general shape of the CFE spectra is well described by the simplified expression $\Phi_F^{(01\bar{2}10)}$ (Table II). The results of the simplified calculation also confirm the fact that the structure observed near 2.45 eV comes from the presence of the Au sandwich layers, giving the correction factor Φ_{FC}.

The effect of light reflection at the interfaces of the Co layer can enhance the CFE in some photon energy ranges[20] because of the nonreciprocal light propagation compared with a single pass effect. This enhancement[20,53] is well revealed in Fig. 11 plotting the variation of the quotient of the specific Faraday rotation per unit length for the Co(t)/Au (25 nm)/*float glass* structure by that of a bulk Co sample. It is also confirmed from the simplified expressions (Table II), the above quantity tending towards $N_{Co}N_{Au}^{-1}$ when $t_2\rightarrow 0$ and for relatively large buffer and overlayer thicknesses. At high Co thicknesses the contribution of the multiple waves reflected in the Co film to the CFE decreases because of the light absorption in the Co layer and the bulk value is finally reached.

D. Magneto-optical contributions of gold layers and glass substrate

We shall now pay attention to the effects which are rather small but which nevertheless contribute to the measured MO signals. These contributions, proportional to the applied magnetic field, originate from the MO activity of nonferromagntic layers and of the float glass substrate.[20,32] A full understanding of the origin of these contributions is important if one wishes to emphasize the consequences of the layered structure on the optical and magneto-optical properties, for example, to reveal modifications of the electronic states at interfaces or by confinement.[54,55]

In light transmission the dominating MO contribution, proportional to the external magnetic field, is the well-known Faraday rotation in the glass substrate.[2] In samples with buffer of finite thickness the CPKE will be affected by the Faraday rotation in the glass substrate, but also by the MO effect of the Au sandwich layers.

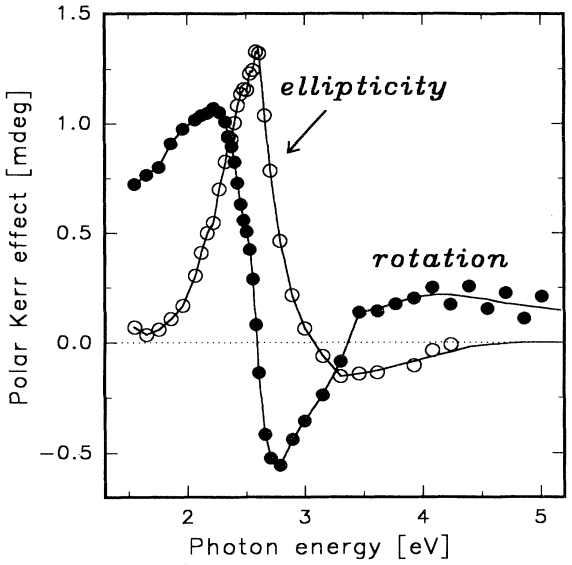

FIG. 12. Polar Kerr rotation (full circles) and ellipticity (empty circles) spectra for a 190 nm thick Au film, measured in a magnetic field of 1.1 T. The lines serve as the guide to the eye.

As reference we carefully measured the PKR and the PKE spectra on the two thickest Au films ($t=160$ and 190 nm), deposited on glass substrates. Since the film thicknesses were large enough, both samples provided the same results, as given for the thickest sample in Fig. 12, within our experimental resolution. Note that the amplitudes of the measured ellipsometric angles are small and of the order of 10^{-3} deg. Our spectra are in a good agreement with the results previously published by Schnatterly[48] who measured the PKE spectrum from which he deduced the PKR using dispersion relations.

The total CPKE contribution of the float glass substrate and of the Au sandwiching layers, obtained by assuming the principle of linear superposition and after subtraction of the effect due to the ferromagnetic Co layer, is compared with the results of calculations in Fig. 13. The contribution of the float glass substrate dominates in the PKR. The peaks near 2.5 and 3.5 eV correspond to the spectroscopic structures appearing in the transmission spectrum of Au (see Fig. 2). On the contrary, since the glass is transparent at the corresponding photon energies, the PKE originates mainly from gold. Note that the modeling of the glass substrate effects is extremely sensitive to a proper choice of the optical and magneto-optical data. This certainly explains the differences between the experimental and calculated spectra (Fig. 13), which look, however, qualitatively similar.

E. MO response variation during the preparation process

A better insight into the optical interactions in Au/Co/Au sandwiches can be handled by the simulation

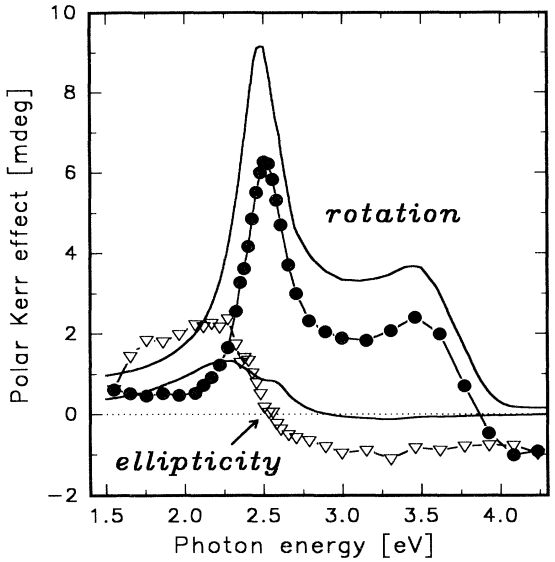

FIG. 13. Nonferromagnetic contributions of the float glass substrate and the Au sandwich layers to polar Kerr rotation (full circles) and polar Kerr ellipticity (empty triangles) spectra, of the Au (5 nm)/Co (0.95 nm)/Au (25 nm)/ *float glass* (1 mm) structure in a magnetic field of 1.1 T, and compared with exact calculations (solid lines).

of the magneto-optical response during the sample preparation process in the ultrahigh vacuum chamber. In Fig. 14 we present the result of a matrix calculation of the PKR in the studied sandwich structure for $t_{Co}=0.8$ nm, as a function of the total deposited metal thickness. Before the deposition large values of the PKR signal are measured due to the glass substrate. The increase of the PKR with photon energy below 3.5 eV reflects the dispersion of FR in float glass. The abrupt decrease between 3.5 and 4 eV is related to the absorption in the float glass substrate, as shown in the inset of Fig. 2. This theoretical dispersion is in very good agreement with the results of our auxiliary experiments. During the deposition of a 25 nm thick Au buffer layer the PKR decreases and the spectrum is modified with respect to the transmission of Au. This results in a decrease of the PKR peak at 3.5 eV with the appearance of a new structure near the plasma edge energy of Au in the vicinity of 2.45 eV. When the Au buffer layer deposition is finished the shape of PKR spectrum is similar to that reported in Fig. 13. During the deposition of the Co layer a negative peak appears in the PKR spectrum in agreement with Eq. (34), as it has been already discussed. The deposition of an Au overlayer, up to a thickness of 5 nm, reduces the value of the PKR, because of the light absorption effect.

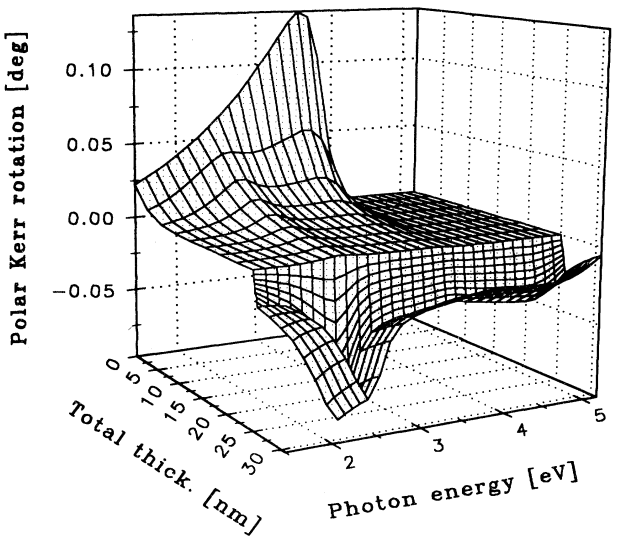

FIG. 14. Simulation of the development of the MO polar Kerr rotation spectrum during the deposition of the Au (5 nm)/Co (0.8 nm)/Au *buffer* (25 nm) structure on 1 mm thick float glass substrate, in a magnetic field of 0.15 T.

CONCLUSIONS

Using a new approach, based on the electromagnetic theory we established general expressions of the polar MO observables in light reflection (Kerr effect) and transmission (Faraday effect) in magnetic layered structures. From these expressions we deduced approximate formulas for sandwich thin magnetic-film structures. These analytical formulas are useful for predicting straightforwardly the sensitivity of MO effects to a change of the different layer thicknesses or to a variation of optical parameters. Noncoherent MO light interaction in the thick transparent substrate is also taken into account using an original procedure.

To demonstrate how the theoretical predictions can be applied to a specific system we carried out precise spectroscopic MO experiments both in polar Kerr and Faraday geometry on well characterized Au/Co/Au sandwiches with perpendicular magnetic anisotropy, deposited on a float glass substrate. To analyze in details the origin of the MO effects in this system we performed spectroscopic experiments in different magnetic fields and carried out auxiliary optical and magneto-optical measurements on Au/Co/Au sandwiches, Au and Co films and float glass substrates.

The trends in the variation of MO effects with the buffer, magnetic layer or overlayer thicknesses are well explained by our simple analytical expressions. The limits of these expressions were discussed. In particular the dependence of the magnitude of MO effects on Co thicknesses is not always exactly linear even for small Co layer thicknesses, especially in the vicinity of the Au plasma edge energy.

In the polar Kerr configuration the shape of the MO spectrum is mainly affected by the optical properties of the buffer layer, whereas the Au overlayer absorption reduces the MO effect. In the Faraday configuration each Au layer plays practically the same role. Variation in the optical properties of gold, but not so much its thickness strongly affect the shape of the Faraday effect spectra.

The MO contribution of the glass substrate and of the Au sandwich layers, proportional to the applied field, has

been measured and evaluated. This is of importance for further evidence of new MO effects which are not predicted by the electromagnetic theory using bulk optical and magneto-optical parameters instead of appropriate ones for confined structures.[54,55]

On the experimental side we have shown that the essential features can be analyzed by the simplified model. We have used two ways to simplify the exact model. The first one is the approximation of the ultrathin magnetic layer. This approximation is not suitable for precise evaluation of the MO effects, but it is very useful to explain the trends in the MO response of the system. The second possibility is based on the simplification of the structure itself. We have shown that even a very simple structure consisting of an ultrathin magnetic film deposited on a thick buffer can be employed to describe qualitatively the CPKE spectra in the sandwich system. When building up the system, starting from such simple structure, more and more features may be precisely explained, as for example the variation of the MO effect with the overlayer and buffer layer thicknesses.

The advantage of our new approach is based on the fact that for a given structure the exact analytical expressions can be simply obtained. After that the level of their simplification can be chosen with respect to the studied effect. This universality of the model and its relative simplicity makes this approach powerful for future MO studies of ultrathin-magnetic-film systems, especially when estimating the consequences of subtle modifications in the structure, for example for taking into account the role of the fine structure at the interfaces. A similar type of treatment could be extended in the future to the case of magneto-optics in longitudinal and transverse configurations for layered systems with in-plane magnetization.

ACKNOWLEDGMENTS

We thank P. Beauvillain and C. Chappert for fruitful discussions and R. Cowburn for critical reading of the manuscript. The Grant Agency of the Czech Republic (GAČR 202/93/2427) and the support of KONSTRUKTIS Praha, Ltd. are gratefully acknowledged. One of us (M.N.) would like to thank the Laboratoire de Physique des Solides, Université Paris-Sud for its kind hospitality and the French Ministère de l'Enseignement Superieur et de la Recherche for financial support. We acknowledge M. Richter and R. Šilha for technical assistance.

[1]J. P. Renard, J. Mater. Sci. Technol. **9**, 1 (1993).
[2]J. Ferré, in *Magnetism, Magnetic Materials and Their Applications,* edited by F. Leccabue and J. L. Sanches Llamazares (IOP, Bristol, 1992), p. 167.
[3]T. Shinjo, Surf. Sci. Rep. **12**, 49 (1991).
[4]S. D. Bader, in Proc. IEEE **78**, 909 (1990).
[5]J. W. M. de Jonge, P. J. H. Bloemen, and F. J. A. den Broeder, in *Ultrathin Magnetic Structures II,* edited by B. Heinrich and J. A. C. Bland (Springer-Verlag, Berlin, in press), Chap. 1.3.
[6]B. Heinrich and J. F. Cochran, Adv. Phys. **42**, 523 (1993).
[7]C. Chappert and P. Bruno, J. Appl. Phys. **64**, 5736 (1988).
[8]R. Allenspach, M. Stampanoni, and A. Bischof, Phys. Rev. Lett. **65**, 3344 (1990).
[9]J. Pommier, P. Meyer, G. Pénissard, J. Ferré, P. Bruno, and D. Renard, Phys. Rev. Lett. **65**, 2054 (1990).
[10]W. R. Bennett, W. Schwarzacher, and W. F. Egelhoff, Jr., Phys. Rev. Lett. **65**, 3169 (1990).
[11]S. T. Purcell, W. Folkerts, M. T. Johnson, N. W. E. McGee, K. Jager, J. aan de Stegge, W. B. Zeper, W. Hoving, and P. Grünberg, Phys. Rev. Lett. **67**, 903 (1991).
[12]Z. Q. Qiu, J. Pearson, and S. D. Bader, Mod. Phys. Lett. **6**, 839 (1992).
[13]V. Grolier, D. Renard, B. Bartenlian, P. Beauvillain, C. Chappert, C. Dupas, J. Ferré, M. Galtier, E. Kolb, M. Mulloy, J. P. Renard, and P. Veillet, Phys. Rev. Lett. **71**, 3023 (1993).
[14]N. M. Baibich, J. M. Broto, A. Fert, F. Nguyen Van Dau, F. Petroff, P. Eitenne, G. Creuzet, A. Friederich, and J. Chazelas, Phys. Rev. Lett. **61**, 2472 (1988).
[15]C. Dupas, J. P. Renard, J. Seiden, E. Vélu, and D. Renard, J. Appl. Phys. **63**, 4300 (1988).
[16]S. S. P. Parkin, N. More, and K. P. Roche, Phys. Rev. Lett. **64**, 2304 (1990).
[17]B. Dieny, J. Magn. Magn. Mater. **136**, 335 (1994).
[18]S. D. Bader and E. R. Moog, J. Appl. Phys. **61**, 3729 (1987).
[19]Z. Q. Qiu, J. Pearson, and S. D. Bader, Phys. Rev. B **46**, 8195 (1992).
[20]J. Ferré, G. Pénissard, C. Marlière, D. Renard, P. Beauvillain, and J. P. Renard, Appl. Phys. Lett. **56**, 1588 (1990).
[21]M. M. H. Willekens, H. J. M. Swagten, A. M. Duif, P. J. H. Bloemen, R. J. T. van Kempen, S. K. J. Lenczowski, and W. J. M. de Jonge, in *Magnetic Ultrathin Films: Multilayers and Surfaces/Interfaces and Characterization,* edited by B. T. Jonker, S. A. Chambers, R. F. C. Farrow, C. Chappert, R. Clarke, W. J. M. de Jonge, T. Egami, P. Grünberg, K. M. Krishnan, E. E. Marinero, C. Rau, and S. Tsunashima, MRS Symposia Proceedings No. 313 (Materials Research Society, Pittsburgh, 1993), p. 129.
[22]P. Yeh, Surf. Sci. **96**, 41 (1980).
[23]Š. Višňovský, Czech. J. Phys. B **36**, 625 (1986).
[24]M. Mansuripur, J. Appl. Phys. **67**, 6466 (1990).
[25]R. Atkinson, J. Magn. Magn. Mater. **95**, 61 (1991).
[26]G. Traeger, L. Wenzel, and A. Hubert, Phys. Status Solidi **131**, 201 (1992).
[27]P. Beauvillain, A. Bounouh, C. Chappert, R. Mégy, S. Ould-Mahfoud, J. P. Renard, P. Veillet, D. Weller, and J. Corno, J. Appl. Phys. **76**, 6078 (1994).
[28]J. Zak, E. R. Moog, C. Liu, and S. D. Bader, J. Magn. Magn. Mater. **89**, 107 (1990).
[29]J. Zak, E. R. Moog, C. Liu, and S. D. Bader, J. Magn. Magn. Mater. **88**, L261 (1990).
[30]E. R. Moog, C. Liu, S. D. Bader, and J. Zak, Phys. Rev. B **39**, 6949 (1989).
[31]W. A. McGahan and J. A. Woollam, Appl. Phys. Commun. **9**, 1 (1989).
[32]Š. Višňovský, M. Nývlt, V. Prosser, J. Ferré, G. Pénissard, D.

Renard, and G. Sczigel, J. Magn. Magn. Mater. **128**, 179 (1993).
[33]J. Ferré, M. Nývlt, G. Pénissard, V. Prosser, D. Renard, and Š. Višňovský, J. Magn. Magn. Mater. (to be published).
[34]Š. Višňovský, Czech. J. Phys. **41**, 663 (1991).
[35]R. M. A. Azzam and N. M. Bashara, *Ellipsometry and Polarized Light* (North-Holland, Amsterdam, 1977).
[36]R. Atkinson and P. H. Lissberger, Appl. Opt. **31**, 6076 (1992).
[37]Š. Višňovský, V. Prosser, and R. Krishnan, J. Appl. Phys. **49**, 403 (1978).
[38]C. Cesari, J. P. Faure, and G. Nihoul, J. Magn. Magn. Mater. **78**, 296 (1989).
[39]N. Mliki, K. Abdelmoula, G. Nihoul, C. Marlière, and D. Renard, Thin Solid Films **224**, 14 (1993).
[40]C. Marlière, D. Renard, and J. P. Chauvineau, Thin Solid Films **201**, 317 (1991).
[41]D. Renard and G. Nihoul, Philos. Mag. **55**, 75 (1987).
[42]N. Mliki, D. Renard, and G. Nihoul (unpublished).
[43]N. Mliki, D. Renard, M. Galtier, and G. Nihoul, Microsc. Microanal. Microstruct. **3**, 55 (1992).
[44]O. Cermáková and Š. Višňovský, Czech. J. Phys. **36**, 537 (1986).
[45]P. B. Johnson and R. W. Christy, Phys. Rev. B **9**, 5056 (1974).
[46]Š. Višňovský, M. Nývlt, M. Pařízek, P. Kielar, V. Prosser, and R. Krishnan, IEEE Trans. Magn. **29**, 3390 (1993).
[47]H. Brändle, D. Weller, J. C. Scott, S. S. P. Parkin, and C. J. Lin, IEEE Trans. Magn. **28**, 2967 (1992).
[48]S. E. Schnatterly, Phys. Rev. **183**, 664 (1969).
[49]D. Weller, W. Reim, K. Spörl, and H. Brändle, J. Magn. Magn. Mater. **93**, 183 (1991).
[50]R. Atkinson, W. R. Hendren, I. W. Salter, and M. J. Walker, J. Magn. Magn. Mater. **130**, 442 (1994).
[51]Š. Višňovský, M. Nývlt, V. Prosser, R. Atkinson, W. R. Hendren, I. W. Salter, and M. J. Walker, J. Appl. Phys. **75**, 6783 (1994).
[52]R. Krishnan, H. Lassri, M. Nývlt, V. Prosser, D. Rafaja, V. Valvoda, and Š. Višňovský, J. Magn. Magn. Mater. (to be published).
[53]G. Pénissard, Ph.D. thesis, Université de Paris XI, Centre d'Orsay, 1993.
[54]R. Mégy, A. Bounouh, Y. Suzuki, P. Beauvillain, P. Bruno, C. Chappert, B. Lecuyer, and P. Veillet, Phys. Rev. B **51**, 5586 (1995).
[55]A. Carl and D. Weller, Phys. Rev. Lett. **74**, 190 (1995).